Resonant contributions to the electron-impact ionization of sodiumlike chromium

J. B. Qi, C. Y. Chen, Y. Zhao, H. N. Xia, Y. S. Wang*
Institute of Modern Physics, Fudan University, Shanghai 200433, China
(Received 21 August 2001; published 26 February 2002)

Electron-impact-ionization cross sections for Na-like Cr^{13+} have been calculated using semirelativistic distorted-wave Born-exchange approximation. We have included direct ionization, excitation autoionization, and resonant-excitation double-autoionization (REDA) processes in our calculation. The overall agreement between experimental data and our theoretical values is very good. Strong resonant peaks from REDA processes are found, and the REDA processes contribute about 50% and 25% to the average total ionization cross section between 570 and 650 eV and between 650 and 860 eV, respectively. A detailed investigation about the effects of radiative damping and loss channels on the REDA cross section has been carried out. The ionization-rate coefficients of Cr^{13+} are also presented. Besides, we have compared our calculated results of Fe^{15+} to experimental data and other theoretical values for examining the reliability of our calculations.

DOI: 10.1103/PhysRevA.65.032720 PACS number(s): 34.80.Kw

I. INTRODUCTION

Electron-impact-ionization cross sections and ionization-rate coefficients are very important in astrophysics, plasmas, and x-ray laser studies [1,2]. In the past years, experimental and theoretical investigations [3–20] have demonstrated that contributions from indirect processes to the ionization cross sections are very important for multiply charged Na-like ions. The most important indirect process is excitation autoionization (EA) from which the cross sections are about two to four times the direct-ionization cross sections [3–12]. Meanwhile the high-order indirect process, resonant-excitation double autoionization (REDA), can also contribute greatly to the total ionization cross section in some particular resonant-energy regions [4–9,13–20].

To date, the electron-impact-ionization cross sections of several Na-like ions have been measured and calculated. Crossed-beam measurements for ionization cross sections of Mg^{+}, Al^{2+}, and Si^{3+} have been made by Crandall *et al.* [3]. Using an electron-beam-modulation technique, Thomason and Peart [4] have measured the ionization cross sections of Na-like Al^{2+} from threshold to 400 eV, where many apparent resonant peaks were found. Rachafi *et al.* [5] and Zhang *et al.* [6] have reported their measurements of cross sections for electron-impact ionization of Ar^{7+}, and the experimental data in the low-energy region of both experiments show some REDA resonances. By using electron-ion crossed-beam apparatus with an ion source and an ion-storage ring, respectively, Gregory *et al.* and Linkemann *et al.* measured ionization cross sections of Ti^{11+} [7], Cr^{13+} [7], and Fe^{15+} [8,9]. Although the measurements in Ref. [7] for Ti^{11+} and Cr^{13+} do not show clear evidences for the REDA mechanism, some energy ranges for both the ions are likely candidates for experimental and theoretical studies of the REDA effect. Linkemann *et al.* resolved the debate about the influence of resonant processes on the electron-impact-ionization cross section of Fe^{15+} by revealing the rich structure using precision measurement. Schneider *et al.* [10] have measured the electron-impact-ionization cross section of Xe^{43+} employing the electron-beam ion trap (EBIT).

Using a unified *R*-matrix method considering REDA and READI (resonant-excitation auto-double-ionization) processes Teng has calculated the cross section for electron-impact ionization of Ar^{2+} [13]. Chen and co-workers have performed detailed calculations of ionization cross sections of Ar^{7+} [14], Fe^{15+} [9,15], Se^{23+} [16], Kr^{25+} [17], and Xe^{43+} [17,18] considering REDA processes using relativistic distorted-wave methods. They concluded that the REDA processes contribute about 10–30 % to the average total ionization cross sections. Tayal and co-worker have studied the REDA processes of Na-like ions Ar^{7+} [19] and Fe^{15+} [20] employing the close-coupling method. Their results show many REDA fluctuations in the resonant-energy region. Using the Breit-Pauli distorted-wave method Linkemann *et al.* have calculated the electron-impact-ionization cross section of Fe^{15+} [9] including REDA processes.

In this paper, we have calculated the electron-impact-ionization cross section of Na-like Cr^{13+} including REDA processes using a semirelativistic distorted-wave Born-exchange (DWBE) approximation method. This approach has been applied successfully in our previous works to obtain the ionization cross sections of the H-, He-, Li-, Ne-, and Na-like isoelectronic sequences [21–24], where the excitation autoionization cross sections for Li- and Na-like ions are included. Our calculated results are in good agreement with the overall magnitude of the experimental cross sections. Besides, we have studied in detail the contributions to REDA from the different intermediates and examined the effects of radiative decay and loss channels on REDA cross sections for Na-like Cr^{13+}. The contribution of REDA to the ionization-rate coefficient is also discussed. Over the past years, the electron-impact-ionization cross section of Fe^{15+} has received particular attention in experiment and theoretical calculations. To show the reliability of the calculations, we present the comparison of our calculated results for Fe^{15+} with the experimental data and other theories at the end of this work.

*Corresponding author. Email address: yswang@fudan.edu.cn

 ©2002 The American Physical Society

II. THEORETICAL METHOD

Our calculational procedures of the direct-ionization and excitation-autoionization cross sections have been described in detail in Refs. [21,22]. We have even studied systematically the REDA cross sections of Li-like ions [25]. The REDA process included in our present calculations is shown schematically below:

$$e+1s^22l^83s\rightarrow 1s^22l^73snln'l'\rightarrow 1s^22l^73sn''l''+e \\ \rightarrow 1s^22s^22p^6+e+e. \qquad (1)$$

Assuming that the direct- and indirect-ionization processes are independent, the total ionization cross section is then given by

$$Q_{\rm tot}=Q_d+\sum_j Q_{\rm exc}(j)B_j^a+\sum_j Q_j^{\rm cap}B_j^{\rm DA}, \qquad (2)$$

where Q_d is the direct-ionization cross section, $Q_{\rm exc}(j)$ and $Q_j^{\rm cap}$ are excitation and dielectronic-capture cross sections, respectively; and B_j^a and $B_j^{\rm DA}$ are the branching ratios for the single and sequential double Auger emission, respectively.

The single and double Auger branching ratios can be written as

$$B_j^a=\frac{\Sigma_m A_{jm}^a}{\Sigma_m A_{jm}^a+\Sigma_k A_{jk}^r} \qquad (3)$$

and

$$B_j^{\rm DA}=\sum_d \left(\frac{A_{jd}^a}{\sum_{d'} A_{jd'}^a+\sum_k A_{jk}^r}\,\frac{\sum_f A_{df}^a}{\sum_{f'} A_{df'}^a+\sum_{k'} A_{dk'}^r}\right) \qquad (4)$$

in which A_{jm}^a and A_{jk}^r are the Auger- and radiative-transition rates, respectively. These transition rates are calculated using the Hartree-Fock approximation with the relativistic-correction method [26]. In the calculation of branching ratios, we included all possible Auger transitions and electric-dipole radiative decays with change of principle quantum number (i.e., $\Delta n\neq 0$).

The cross section $Q_j^{\rm cap}$ captured to level j is calculated from the inverse Auger process [15,27],

$$Q_j^{\rm cap}(E)=\frac{\pi^2\hbar^3 g_j}{2m_eE_jg_i}A_{ji}^a\delta(E-E_j), \qquad (5)$$

where E_j is Auger energy, g_i $(=2J_i+1)$ and g_j $(=2J_j+1)$ are the statistical weight before and after the incident electron is captured.

For the REDA processes, we carried out explicit calculations for resonant states from the intermediate states $1s^22s^22p^53s4lnl'$ $(n=4-7)$, $1s^22s2p^63s4lnl'$ $(n=4-7)$, $1s^22s^22p^53s3lnl'$ $(n=6-10)$, $1s^22s2p^63s3lnl'$ $(n=6-10)$, and $1s^22s^22p^53s5l5l'$. Extrapolation to $n=30$ was accomplished using the n^{-3} scaling [15] for the Auger-transition rates.

With the total cross section, we can get the ionization-rate coefficient, which is defined as

$$\alpha=\int_0^\infty \nu f(\nu)Q_{\rm tot}(\nu)d\nu, \qquad (6)$$

where $f(\nu)$ is the velocity distribution of the electrons. Usually a Maxwellian distribution of velocities is assumed. The ionization-rate coefficient from direct-ionization and excitation-autoionization processes for Na-like Cr^{13+} have been calculated in our previous paper [24]. Here the cross sections from REDA processes have been included in $Q_{\rm tot}(\nu)$.

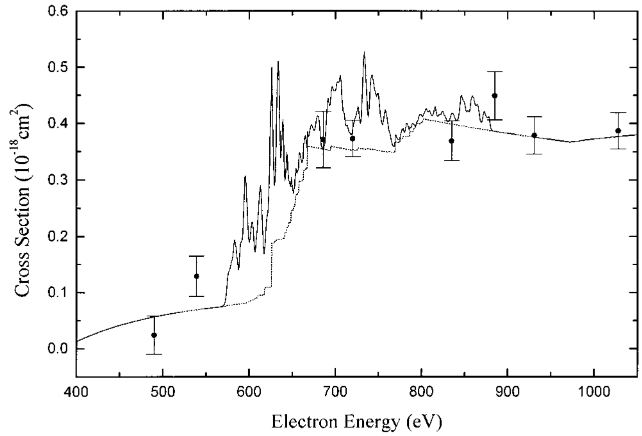

FIG. 1. Total ionization cross section for Cr^{13+}. The dashed curve shows the direct- and excitation-autoionization cross sections. The solid curve represents the total ionization cross section including REDA contributions. The black dots with error bars are experimental data from [5].

III. RESULTS AND DISCUSSION

For the REDA processes, we have done a comprehensive calculation including more than 20 000 intermediate autoionizing levels taking into account the effects of radiative damping and loss channels. The REDA resonances were convoluted with a Gaussian of 2 eV in width to simulate the experiments of Gregory *et al.* [7]. Our results and experimental data are shown in Fig. 1. It can be seen from Fig. 1 that the calculated values agree quite well with the experimental data in magnitude over the entire energy region. The strong peaks from REDA processes exist in the interval from 570 to 750 eV, where, unfortunately, there are only two experimental points. It can be seen that the REDA processes contribute about 50% and 25% to the average total ionization cross section between 570 and 650 eV and between 650 and 860 eV, respectively.

In Fig. 2, we show the total REDA cross sections for Cr^{13+} in detail. It can be seen that most of the prominent features in the ionization cross sections are due to the combined effects of REDA resonances. The resonances below

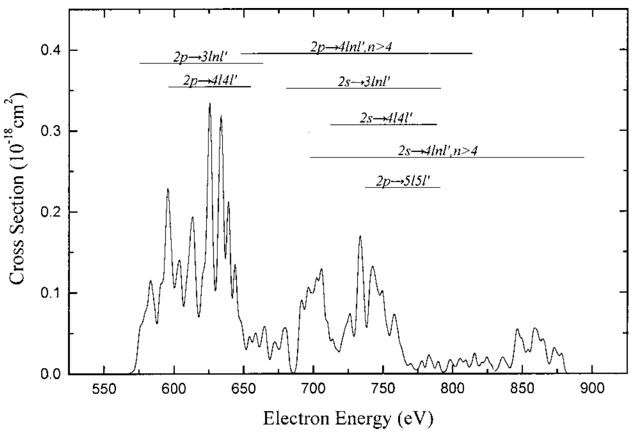

FIG. 2. Total REDA cross sections as a function of electron energy.

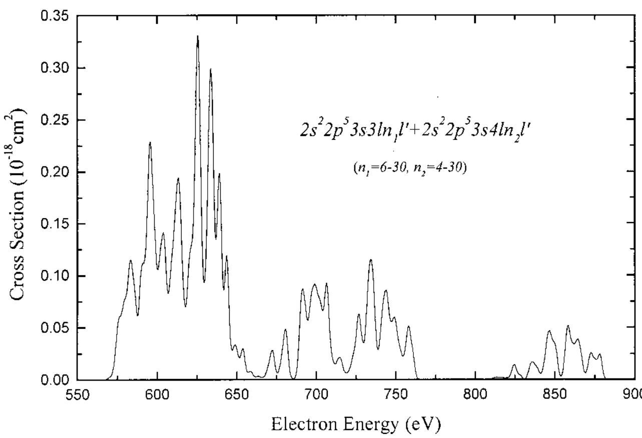

FIG. 3. REDA cross sections from $2s^2 2p^5 3s3ln_1l'$ ($n_1 = 6-30$) and $2s^2 2p^5 3s4ln_2l'$ ($n_2 = 4-30$) states as functions of electron energy.

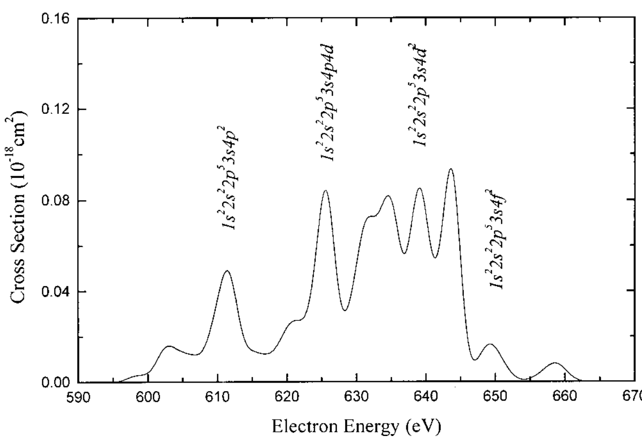

FIG. 4. REDA cross sections from four autoionizing configurations in the $2l^{-1}3s4l4l'$ state.

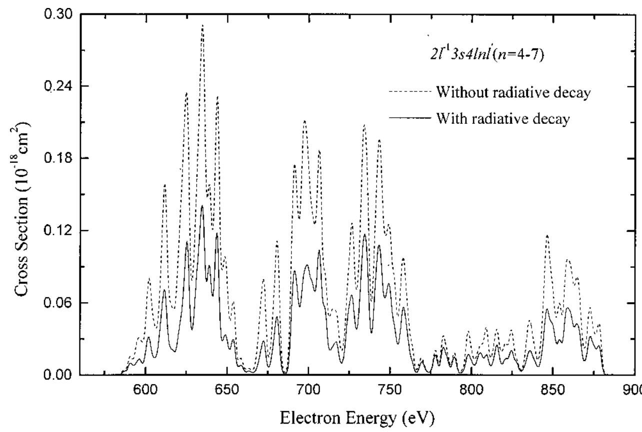

FIG. 5. REDA cross sections from the $2l^{-1}3s4lnl'$ ($n = 4-7$) as functions of energy. The solid and dotted curves indicate the results with and without radiative damping, respectively.

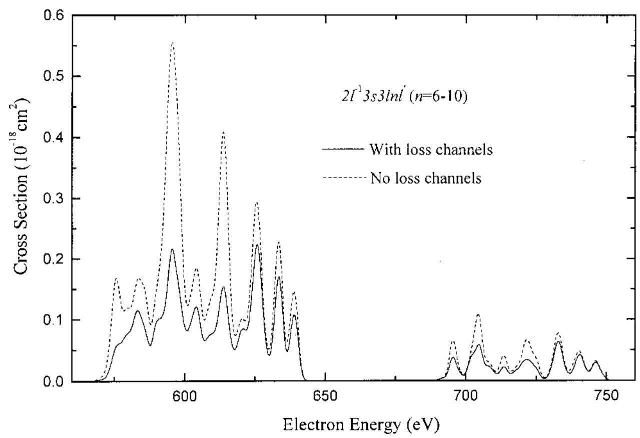

FIG. 6. The effects of loss channels on the REDA cross sections for the $2l^{-1}3s3lnl'$ ($n = 6-10$) intermediate states. The solid and dashed curves are the cross sections with and without the effects of loss channels, respectively.

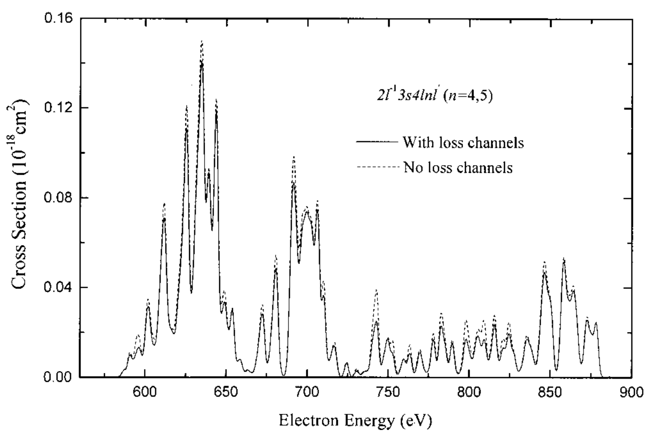

FIG. 7. The effects of loss channels on the REDA cross sections for the $2l^{-1}3s4lnl'$ ($n = 4,5$) intermediate states. The solid and dashed curves are the cross sections with and without the effects of loss channels, respectively.

TABLE I. Radiative damping influence on REDA cross sections for the $2s2p^63s4s5p$ intermediate state of Cr^{13+} at each Auger energy. The number in brackets denotes the power of 10.

Energy (eV)	J	Cross section (cm^2) not radiative	Cross section (cm^2) radiative in 2nd step	Cross section (cm^2) radiative in both steps
773.952	1.0	0.1866[−23]	0.1546[−23]	0.1514[−23]
774.025	2.0	0.1214[−22]	0.5295[−23]	0.5172[−23]
774.212	3.0	0.0000[+00]	0.0000[+00]	0.0000[+00]
774.476	2.0	0.1329[−21]	0.9480[−22]	0.9006[−22]
774.530	1.0	0.7078[−22]	0.6052[−22]	0.5739[−22]
774.553	0.0	0.2181[−22]	0.2037[−22]	0.1930[−22]
777.646	0.0	0.4773[−20]	0.4281[−20]	0.4228[−20]
777.703	1.0	0.1427[−19]	0.1171[−19]	0.1156[−19]
777.875	2.0	0.2289[−19]	0.1736[−19]	0.1713[−19]
778.515	1.0	0.1757[−19]	0.1590[−19]	0.1562[−19]
782.229	1.0	0.2193[−20]	0.2133[−20]	0.2094[−20]
782.369	0.0	0.1523[−20]	0.1451[−20]	0.1428[−20]
782.514	1.0	0.4332[−20]	0.4080[−20]	0.4010[−20]
782.652	2.0	0.7819[−20]	0.7238[−20]	0.7116[−20]

620 eV mainly arise from intermediate states $2s^22p^53s3lnl'$ ($n=6,7$). The strong peaks between 620 and 670 eV are due to $2s^22p^53s4l4l'$ and $2s^22p^53s3lnl'$ ($n\geqslant 8$) resonances. For electron energy $E\geqslant 670$ eV, $2s^22p^53s4lnl'$ ($n\geqslant 5$), $2s2p^63s3lnl'$, $2s2p^63s4lnl'$, and $2s^22p^53s5l5l'$ states are responsible for the resonance structure. The REDA cross sections from the intermediate states $2s^22p^53s4lnl'$ ($n=4-30$) and $2s^22p^53s3lnl'$ ($n=6-30$) are displayed in Fig. 3. Comparing Fig. 3 with Fig. 2, it can be seen that these Rydberg series contribute most of the REDA processes. In order to make out the contributions of different autoionizing configurations to the intermediate states, we present in Fig. 4 the cross sections from four autoionizing configurations, which play a dominant role in contributing to the REDA processes in the $2p^53s4l4l'$ state.

Radiative damping plays an important role in calculations of EA and REDA. Figure 5 shows the REDA cross section from the $2l^{-1}3s4lnl'$ ($n=4-7$). The solid and dashed curves are cross sections with and without radiative decay, respectively. From Fig. 5, it can be seen that radiative damping can decrease the total REDA cross section by a factor of 2. In Table I the energy positions and cross sections of the first step and the second step from the intermediate state $2s2p^63s4s5p$ are listed. Table I shows that Auger transitions completely dominate the decay process in the first step and the reduction of autoionization cross section mainly occurs in the second step.

The loss channels also have a significant effect on the calculated REDA cross section. In the first step of the autoionization processes, the dielectronic capture states can

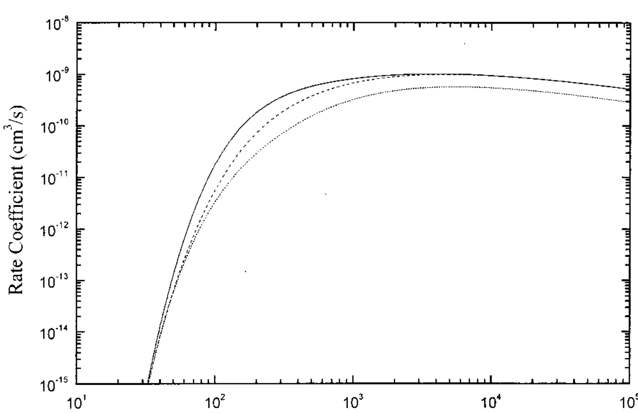

FIG. 8. Ionization-rate coefficients of Cr^{13+}. The dotted line includes only direct ionization. The dashed curve includes contributions from direct ionization and excitation autoionization. The solid line involves contributions from direct ionization, excitation autoionization, and REDA.

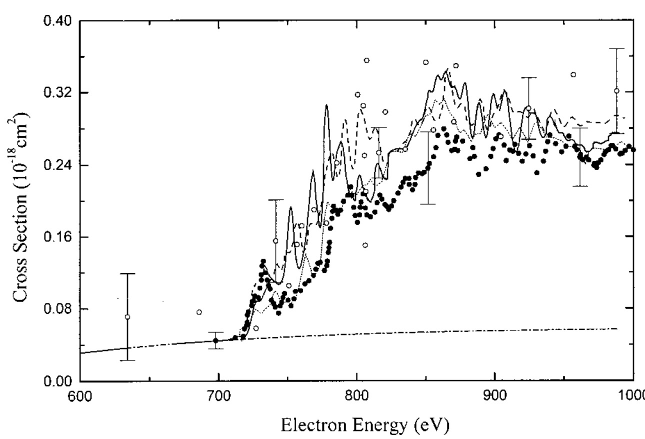

FIG. 9. Ionization cross sections of Fe^{15+} from our results, the experimental data, and theoretical results. Data of Linkemann *et al.* [9] are indicated by solid circles, measurements of Gregory *et al.* [8] by open circles. The solid curve is our theoretical value. The dashed curve and dotted curve are the calculated results from Chen *et al.* [15] and Linkemann *et al.* [9], respectively. The dashed-dotted curve is our result for the direct-ionization cross section.

decay to an excited bound state, which stabilizes by radiative damping, so the process does not contribute to the REDA cross section, and thus represents a loss to the ionization channels. Figure 6 shows that the loss channels reduce the $2l^{-1}3s3lnl'$ ($n=6-10$) REDA cross sections by a factor of 1–3 in the entire energy range. However our calculations show that the effect of loss channels on the $2l^{-1}3s4lnl'$ ($n=4,5$) state (See Fig. 7) is quite small.

By using the formula (6) the ionization-rate coefficients of Cr^{13+} are calculated and plotted in Fig. 8, from which we can see that in the region of the electron temperature, 40–1000-eV REDA processes greatly enhance the rate coefficients by a factor of 1–2.5.

Many experiments and theoretical calculations have been done on the cross section of Na-like Fe^{15+}. In Fig. 9 we present our calculation for the total cross section of Fe^{15+} including REDA processes. Each REDA resonance is convoluted with a experimental Gaussian of width $0.17\sqrt{E}$ eV [9]. It can be seen that our results are in good agreement with the overall magnitude of experimental cross sections and other theoretical values. However the theories disagree with each other and with the experiments with respect to the fine details of the ionization. As pointed in Ref. [9], the major differences arise in two ways. First, the REDA cross section sits on a rapidly varying EA contribution. Second, there are contributions from many different series. Small uncertainties in the energy position of the different autoionizing levels, and hence the resonances attached to them, can give rise to large differences in the superposed results.

IV. CONCLUSIONS

We have calculated the REDA cross section for Cr^{13+}. The total ionization cross section including the direct-ionization, excitation-autoionization, and resonant-excitation double-autoionization processes is found to be in good agreement with the experimental data [7]. Strong resonant peaks from REDA exist in the energy range from 570 to 750 eV. It is important to include REDA processes in calculating electron-impact-ionization cross sections. Radiative damping and loss channels play significant roles in calculating the REDA cross sections. New precision measurements of Cr^{13+} are needed to compare these results with the theoretical results.

ACKNOWLEDGMENTS

This work was supported by the National Natural Science Foundation of China, Project No. 10104005, National High-Tech ICF Committee in China, the Chinese Research Association of Atomic and Molecular Data, and the Research Foundation of Zhonglu Corporation.

[1] T. D. Mark and G. H. Dunn, *Electron Impact Ionization* (Springer, Wien, 1986).
[2] J. A. Stephens and J. Botero, *International Bulletin on Atomic and Molecular Data for Fusion* (IAEA, Vienna, 1995).
[3] D. H. Crandall, R. A. Phaneuf, R. A. Falk, D. S. Belic, and G. H. Dunn, Phys. Rev. A **25**, 143 (1982).
[4] J. W. G. Thomason and B. Peart, J. Phys. B **31**, L201 (1998).
[5] S. Rachafi, D. S. Belie, M. Duponchelle, J. Jureta, M. Zambra, Zhang Hui, and P. Defrance, J. Phys. B **24**, 1037 (1991).
[6] Y. Zhang, C. B. Reddy, R. S. Smith, D. E. Golden, D. W. Mueller, and D. C. Gregory, Phys. Rev. A **45**, 2929 (1992).
[7] D. C. Gregory, L. J. Wang, B. R. Swenson, H. Sataka, and S. J. Chantgenne, Phys. Rev. A **41**, 6512 (1990).
[8] D. C. Gregory, L. J. Wang, F. W. Meyer, and K. Rinn, Phys. Rev. A **35**, 3256 (1987).
[9] J. Linkemann, A. Muller, J. Kenntner, D. Habs, D. Schwalm, A. Wolf, N. R. Badnell, and M. S. Pindzola, Phys. Rev. Lett. **74**, 4173 (1995).
[10] D. Schneider *et al.*, Phys. Rev. A **42**, 3889 (1990).
[11] D. C. Griffin, M. S. Pindzola, and C. Bottcher, Phys. Rev. A **36**, 3642 (1987).
[12] M. S. Pindzola, D. M. Mitnik, J. A. Shaw, D. C. Griffin, N. R. Badnell, H. P. Summers, and D. R. Schultz, Phys. Scr. **57**, 514 (1998).
[13] H. G. Teng, J. Phys. B **33**, L553 (2000).
[14] K. J. Reed and M. H. Chen, Phys. Rev. A **54**, 2967 (1996).
[15] M. H. Chen, K. J. Reed, and D. L. Moores, Phys. Rev. Lett. **64**, 1350 (1990).
[16] M. H. Chen, K. J. Reed, and D. M. McWilliams, Phys. Rev. A **52**, 2881 (1995).
[17] M. H. Chen and K. J. Reed, Phys. Rev. A **47**, 1874 (1993).
[18] K. J. Reed, M. H. Chen, and D. L. Moores, Phys. Rev. A **42**, 5315 (1990).
[19] S. S. Tayal and R. J. W. Henry, Phys. Rev. A **39**, 3890 (1989).
[20] S. S. Tayal, Phys. Rev. A **49**, 2651 (1994).
[21] D. Fang, W. Hu, C. Y. Chen, Y. Wang, F. Lu, J. Tang, and F. Yang, At. Data Nucl. Data Tables **61**, 91 (1995).
[22] C. Y. Chen, W. Hu, D. Fang, Y. Wang, F. Yang, and H. Teng, At. Data Nucl. Data Tables **64**, 301 (1996).
[23] C. Y. Chen, Z. X. Teng, S. X. Yan, Y. Wang, and F. Yang, At. Data Nucl. Data Tables **70**, 255 (1998).
[24] C. Y. Chen, J. B. Qi, Y. S. Wang, F. J. Yang, X. J. Xu, and Y. S. Sun, At. Data Nucl. Data Tables **79**, 65 (2001).
[25] Z. X. Teng, C. Y. Chen, Y. S. Wang, and X. J. Xu, Acta Phys. Sin. **48**, 1858 (1999).
[26] R. D. Cowan, *The Theory of Atomic Structure and Spectre* (University of California Press, Berkeley, 1981).
[27] K. T. LaGuttuta and Y. Hahn, Phys. Rev. A **24**, 2273 (1981).